ChemComm

Accepted Manuscript

This article can be cited before page numbers have been issued, to do this please use: J. Yu, Q. Yan, W. Chen, A. Jain, J. Neaton and K. Persson, *Chem. Commun.*, 2015, DOI: 10.1039/C4CC08111K.

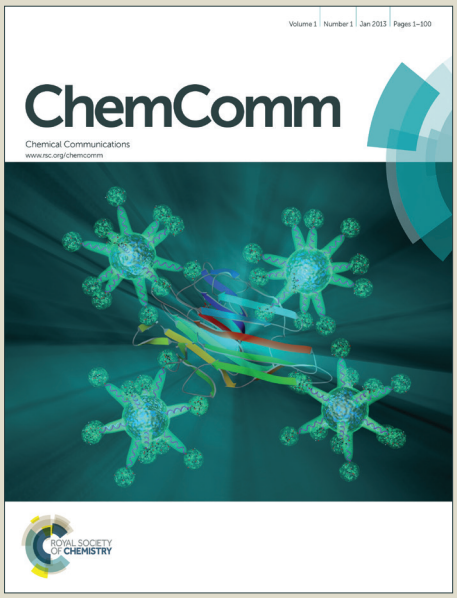

ROYAL SOCIETY OF CHEMISTRY

www.rsc.org/chemcomm

View Article Online
DOI: 10.1039/C4CC08111K

ChemComm

RSCPublishing

COMMUNICATION

First-principles study of electronic structure and photocatalytic properties of $MnNiO_3$ as an alkaline oxygen-evolution photocatalyst

Cite this: DOI: 10.1039/xoxxoooooox

Received ooth October 2014,
Accepted ooth xxxxxxx 20xx

DOI: 10.1039/xoxxoooooox

www.rsc.org/

Jie Yu [a, b, c], Qimin Yan [c, d], Wei Chen [b], Anubhav Jain [b], Jeffrey B. Neaton [c, d, e] and Kristin A. Persson [b, *]

We present a first-principles study of $MnNiO_3$, a promising oxygen-evolution photocatalyst. Using density functional theory with the PBE+U functional and the screened hybrid functional of Heyd, Scuseria, and Ernzerhof (HSE), we compute and analyze the ground-state geometry and electronic structure. We find that $MnNiO_3$ is a ferrimagnetic semiconductor with an indirect band gap, consistent with experimental observations. We also predict that $MnNiO_3$ has promising band edge positions relative to the vacuum, with potential to straddle the hydrogen evolution reaction (HER) and oxygen evolution reaction (OER) redox potentials in aqueous solution. A detailed analysis of the band structure and density of states provides a clear explanation for why $MnNiO_3$ has appropriate electronic properties for OER. Furthermore, comprehensive calculations of its Pourbaix diagram suggest that $MnNiO_3$ is stable in alkaline solution at potentials relevant for oxygen evolution.

There are several strict requirements for a functional material in an efficient photocatalytic water splitting system, including band gaps in the visible, band edge positions bracketing the water redox potentials, and long-term electrochemical stability.[1] To enable photocatalytic water splitting, the conduction and valence bands of the photocatalyst material must straddle the redox potentials of the hydrogen evolution reaction (HER) (0 V vs NHE) and oxygen evolution reaction (OER) (1.23 V vs NHE). Earth-abundant metal oxides are a promising class of materials as high activity and low cost photocatalysts due to their high chemical and electrochemical stability.[2, 3] However, the band gaps of these metal oxides are commonly too large to absorb a significant portion of visible light.[4-6]

As one of the earth-abundant metal elements, Mn is known to show strong electrochemical stability in aqueous solutions close to the OER potential.[7, 8] However, the activity of binary Mn oxides for OER is not as high as that of some other metal oxides, such as IrO_2.[9] In a recent experimental work, $NiFe_2O_4$ was reported to be a highly active and robust catalyst for photocatalytic water oxidation. Moreover, the catalytic activity of $NiFe_2O_4$ was found to be two times higher than that of NiO, which has important implications for the exploitation of ternary metal oxides containing earth-abundant metals as efficient oxygen evolution photocatalysts.[10] To overcome the intrinsic limitations of Mn oxides for photocatalytic and optoelectronic applications, it is highly desirable to develop new multi-ternary Mn based oxides with optimal electronic properties and electrochemical stability against electrochemical corrosion and photo corrosion. Recently, $MnNiO_3$ was found to be an efficient photocatalyst for oxygen evolution under visible light with a photosensitizer and a sacrificial oxidant.[11] To the best of our knowledge, the fundamental electronic structure of $MnNiO_3$ has not been explored to explain the improved performance of this ternary compared to its binary counterparts. In particular, its band gap is unknown, as are the roles the Mn and Ni cations play in determining its functional properties. In this work, we present a computational first-principles study of the structure, magnetic properties, electronic structure, and electrochemical stability of $MnNiO_3$, which we hope will guide future development of $MnNiO_3$ based photocatalytic systems.

Our first-principles computations based on density functional theory (DFT) are performed using the Vienna software package (VASP)[12], with the PAW pseudopotentials[13], the generalized gradient approximation (GGA) as implemented by Perdew, Burke and Ernzerhof (PBE)[14], and the screened hybrid functional of Heyd, Scuseria, and Ernzerhof (HSE)[15, 16]. The PBE+U method is used to address the on-site Coulomb interactions in the localized d orbitals by adding an additional Hubbard-type U term, with values of 3.9 eV for Mn and 6.2 eV for Ni as reported for binary metal oxides.[17] The mixing parameter for the Hartree-Fock exchange potential is set to 25%. A 6 × 6 × 6 Monkhorst-Pack k-point mesh for the integrations over the Brillouin zone is used. We use an energy cutoff of 450 eV and spin-polarization is included in all calculations. The bulk unit cell is relaxed with the HSE functional. In treating the surfaces, we use HSE lattice constants but relax surface atomic positions with the PBE+U functional. Performing structural relaxations with this combination of the two functionals has proven to be accurate and

View Article Online
DOI: 10.1039/C4CC08211K ChemComm

efficient to estimate the band edge positions of group-III nitrides.[18] The vacuum layer is set to 20 Å for our surface calculations. We carry out both bulk and surface relaxations until the forces on each atom are less than 0.01 eV/Å. These criteria lead to good convergence of structural and electronic properties.

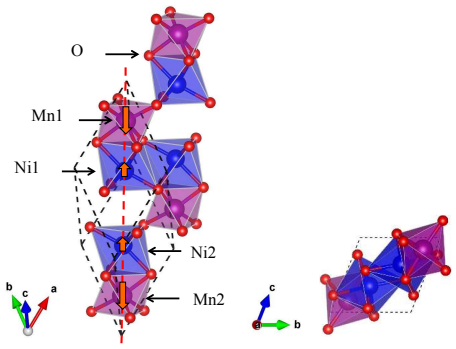

Figure 1 Illustration of $MnNiO_3$ structure in the ferrimagnetic ground state, which was obtained through HSE calculations. Black dash lines indicate the primitive cell. Blue, purple, and red spheres denote the Mn, Ni, and O atoms. The red dashed line is along the rhombohedron body diagonal.

$MnNiO_3$ crystallizes in the same structure as ilmenite ($FeTiO_3$)[19, 20] (space group 148, $R\bar{3}$) with rhombohedral symmetry. The structure of the ilmenite ABO_x is similar to that of Cr_2O_3, where both A and B sites are occupied by Cr atoms.[21] In ilmenite structures, A and B atoms form an AB-BA-AB-BA arrangement with oxygen atom layers stacked along the rhombohedron body diagonal. The primitive cell of rhombohedral $MnNiO_3$ (black dashed line) used in our DFT-HSE calculations is shown in Fig. 1. The Mn and Ni atoms are both surrounded by a distorted oxygen octahedron, with nearest neighbour distances ranging from 1.932 to 1.957 Å for Mn and from 2.029 to 2.141 Å for Ni. The positions of the A, B, and O atoms in the rhombohedral cell of the ilmenite structure can be described with the following Wyckoff positions [19]: metal A: ±u, u, u; metal B: ±v, v, v; oxygens: ±(xyz, zxy, yzx) with the restriction of the oxygen positions as x + y = 2z.[22] We relax the bulk structure with both PBE+U and HSE functionals. Detailed results are shown in Table S1 in the Supplementary Information. The equilibrium lattice parameters and atomic coordinates obtained from our DFT-HSE calculations are in excellent agreement with previous experimental data[19], with deviations of less than 0.5% in lattice constants and 5% in atomic coordinates (Table S2).

Our calculations suggest that the ferrimagnetic phase is the ground state, which is consistent with previous experimental observations.[19, 20, 23-26] The obtained band gaps from PBE+U and HSE calculations are 1.75 eV and 2.98 eV, respectively (Table S3). Detailed study of the magnetic properties of $MnNiO_3$ with PBE+U and HSE methods is provided in the Supplementary Information. Since DFT is well known to underestimate gaps, the quantitative nature of these predictions is necessarily limited. Many-body perturbation theory within the GW approximation can result in more reliable gaps for many inorganic semiconductors,[27] despite its neglect of excitonic effects and electron-phonon interactions; this success can extend, in some cases, to complex oxides.[28, 29] However, DFT can often provide reliable trends in the band gap for oxides at significantly reduced computational cost[30, 31], and empirically, the HSE functional has been shown to lead, in certain cases, to near-quantitative accuracy for the gap for many complex oxides[32]. Thus, here we limit our analysis of the band gap to the DFT level. Although HSE and PBE+U differ significantly in the absolute value of the band gap, the trend remains the same: the band gap for the ferromagnetic state is lowest compared with other magnetic states, and the antiferromagnetic phase with a +-+- configuration exhibits the largest band gap.

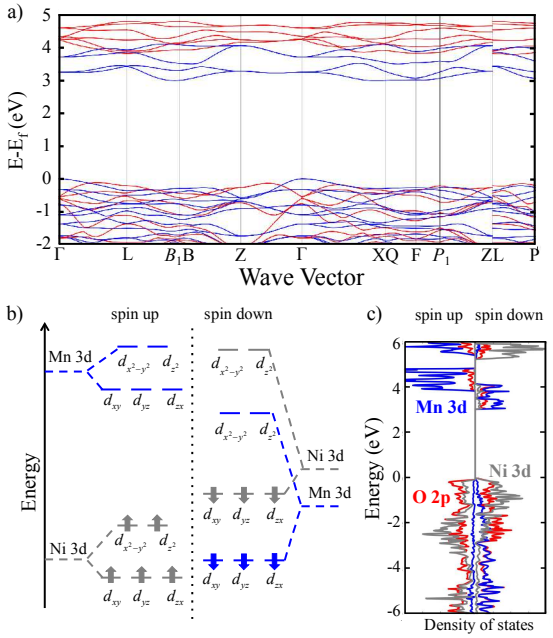

Figure 2 (a) The HSE band structure of $MnNiO_3$. Red and blue colours denote spin up and spin down channels, respectively. (b) The schematic showing the splitting and occupation of d orbitals on Mn (blue) and Ni (grey) atoms in a distorted octahedral environment. (c) Atom projected density of states of $MnNiO_3$. The energy of the highest occupied state is set to 0 eV.

The band structure for $MnNiO_3$ is shown in Fig. 2(a). Ferrimagnetic $MnNiO_3$ is predicted to be an indirect band gap semiconductor. The valence band maximum (VBM) is located at Γ point, while the conduction band minimum (CBM) is at a k-point along the Γ-X direction. Polynomial fits of the energy-momentum relation along the Γ-*L*, Γ-*Z* and Γ-X lines yields effective hole masses of 2.34 m_0 , 0.88 m_0 and 2.71 m_0 respectively. The atom and *l*-projected density of states (DOS) for $MnNiO_3$ are shown in Fig. 2(c). The VBM is mostly composed of Ni 3d and O 2p states. The occupied Mn 3d states in the spin-down channel are located at 1.5 eV below the VBM. O 2p states spread between 0 and -6 eV, with respect to the highest occupied state. Mn 3d states dominate the CBM, with a considerable contribution from O 2p and Ni 3d states in the spin-down channel. As shown in Table S3, the calculated magnetic moments for the ferrimagnetic ground state of $MnNiO_3$ are -2.9 μ_B on Mn atom and +1.7 μ_B on Ni atom, where μ_B is the Bohr magneton. Considering that the electron configurations of Mn and Ni atoms are $3d^5 4s^2$ and $3d^8 4s^2$, the oxidation states of Mn should be 4+ with three d electrons in the spin-down channel while those of Ni atoms should be 2+ with eight d electrons (5 spin up and 3 spin down). Because of the octahedral symmetry of MnO_6 and NiO_6 block, the d states of Mn and Ni are split into e_g and t_{2g} orbitals and the positions of these orbitals, based on the analysis of the site-projected densities of states, are plotted in Fig. 2(b). In the spin-up channel, both t_{2g} and e_g orbitals for Mn atoms are unoccupied (CBM), while both t_{2g} and e_g orbitals for Ni atoms are occupied (VBM). In the spin-down channel, t_{2g} states for both Mn and Ni atoms are occupied while e_g states are both unoccupied. The energies of d states for Ni are higher in energy than those for Mn, which

ChemComm View Article Online
DOI: 10.1039/C4CC08111K COMMUNICATION

results in a VBM mainly composed of Ni t_{2g} and a CBM mainly composed of Mn e_g states. In an approximate one-particle picture neglecting electron-hole correlation effects, one may consider the corresponding optical transitions close to the band gap as charge-transfer transitions, where electrons transferred from Ni to Mn atoms.

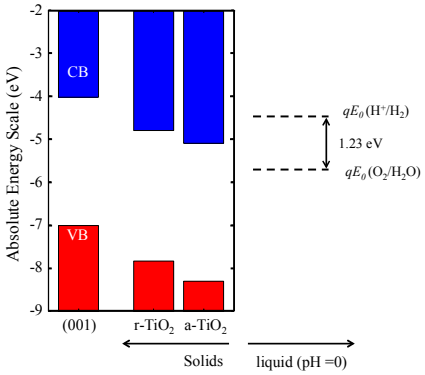

Figure 3 The positions of the VBM (red) and CBM (blue) of $MnNiO_3$ comparing with rutile TiO_2 and anatase TiO_2 relative to the vacuum. The positions of the two water redox potentials at pH = 0 are shown on the right.

To better understand the viability of $MnNiO_3$ for photocatalytic water splitting applications, we examine its band edge energies relative to vacuum, and discuss these energies relative to the redox potentials of water. As band edge energies are, strictly speaking, electron addition and removal energies, self-energy corrections to DFT eigenvalues within, e.g, the GW approximation, are necessary in principle. GW calculations for oxides are challenging, and prior work has shown that DFT calculations with hybrid functionals can provide reliable and in some cases quantitative trends.[18, 33, 34] Here, we provide insight into the band edge energies relative to vacuum in a computationally-efficient manner by combining bulk HSE and PBE+U surface slab calculations of $MnNiO_3$.[18] The generalized Kohn-Sham eigenvalues obtained from a bulk HSE calculation are referenced to the average electrostatic potential of a PBE+U slab calculation.

More concretely, we perform supercell calculations with a surface slab region and a vacuum region. The vacuum level is then defined by the value of the electrostatic potential far away from the surface slab; the "bulk" average electrostatic potential is defined as the macroscopically averaged electrostatic potential in a "bulk" region deep inside the slab. The potential step ΔV between the vacuum and the bulk is then established, and the bulk Kohn-Sham eigenvalues can be referenced to the vacuum. We construct several low-index nonpolar surfaces of $MnNiO_3$ using the surface generation scheme proposed in Ref. [35], carry out surface geometry optimization, and calculate their surface energies. Our calculations predict that the (001) surface has the lowest surface energy. Considering the fact that other low-index surfaces have surface energies more than 60 meV/Å^2 higher, we evaluate only the band edge positions involving the (001) surface. Using the above approach, we predict that the CBM for the (100) surface is located at 4.03 eV below the vacuum while the VBM is at 7.01 eV below the vacuum. As shown in Fig. 3, without considering the solid-liquid interface effects, the CBM and VBM of $MnNiO_3$ straddle the two water reaction levels. Compared with TiO_2[36] (and shown in Fig. 3), the position of VBM for $MnNiO_3$ is higher in energy due to the presence of occupied Ni 3d states. In a realistic photocatalystic system, the relative stability of MnNiO3 surfaces and the band edge positions can be affected by solid-solution interaction. Since the surface energy of the most stable (001) surface is much lower than those of other surfaces by at least 60 meV/ Å^2, we do not expect the solid-solution interaction will change the dominant surface for $MnNiO_3$ in water. Using the method proposed in Ref. [37] and assuming the pH of the point of zero charge for $MnNiO_3$ is between that of MnO_2 (4.5)[38] and NiO (8.2)[39], the band edge positions in aqueous solution at pH = 0 are estimated to be 0.02~0.24 eV closer to vacuum than predicted by our DFT calculations without water. Considering the fact that the offset between the VBM/CBM of $MnNiO_3$ and the OER/HER potential are quite large, the estimated band edge position shifts due to water will not affect our main conclusion that the VBM and CBM of $MnNiO_3$ straddle the two water redox potentials.

Compared with manganese oxide and nickel oxide, the $MnNiO_3$ system has shown better catalytic activity with a higher O_2 production rate.[11] This observation possibly originates from the difference in their electronic structures. It is well known that MnO and NiO are Mott insulators with large band gaps (3.8 eV[40] and 4.0 eV[41] respectively) and localized electronic bands close to the VBM. However, the highest valence band of $MnNiO_3$ has a strongly mixed Ni d and O p character and a large band dispersion, especially along the Γ-Z direction. It suggests a higher hole mobility and possibly lower carrier recombination rates in $MnNiO_3$, which may provide the superior catalytic performance compared to Mn and Ni oxides.

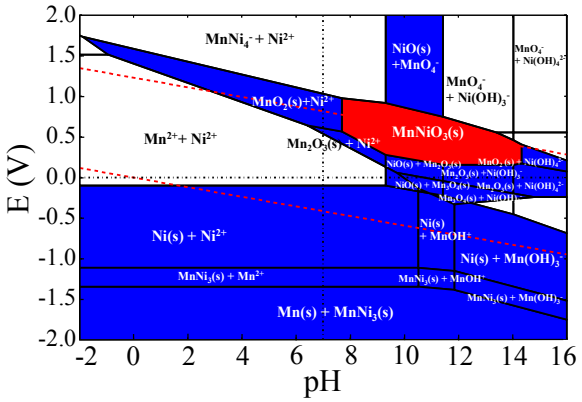

Figure 4 The Pourbaix diagram of 50%-50% Mn-Ni system in aqueous solution, assuming a Mn ion concentration at 10^{-6} mol/kg and a Ni ion concentration at 10^{-6} mol/kg. The upper red dashed line represents the potential for OER, while the lower red dashed line corresponds to the potential for HER. The blue and red regions contain stable solid compounds, while only ions are stable in the white regions.

The stability against electrochemical corrosion and photo-corrosion is a critical issue prohibiting the application of many candidate materials with promising electronic structure properties for water-splitting applications. Hence, for electrochemical corrosion, we employ the analysis of the Pourbaix diagram, as implemented in the Materials Project[42] to assess the stability and feasibility of the Mn-Ni ternary space. The analysis is based on the work of Persson *et al.*[8], where solid and dissolved species are combined in a single-phase diagram to determine the stable species (solids and/or aqueous ions) as a function of pH and potential.[43] Following Ref[8] , the theoretical data obtained with the PBE+U method are used for the total energies of solid phases and experimental data are utilized for the dissolved ions. Based on these energy data, the Pourbaix diagram for Mn and Ni containing species (with the concentrations of Mn and Ni ions set at ~10^{-6} mol/kg) is constructed and shown in Fig. 4. The $MnNiO_3$ is clearly stable –even at fairly alkaline conditions - as evidenced by its large phase space with pH values from 7.5 to 14 and potentials close

View Article Online
DOI: 10.1039/C4CC08211K ChemComm

to the oxygen evolution potential. In this region, the normalized Gibbs free energy of $MnNiO_3$ becomes lower than all the other possible dissolution products and it exists in aqueous solution as a solid.

The understanding of the electrochemical stability of $MnNiO_3$ can be achieved by constructing the Pourbaix diagrams of Mn metal and Ni metal, respectively. From the calculated Pourbaix diagram of Mn (not shown here), we see that MnO_2 is the stable phase close to the OER potential in a large pH range, which is in good agreement with the experimental observation.[44] For Ni based species, the solid phases of Ni compounds only exist in the alkaline region close to the OER potential.[45] We thus expect the appearance of ternary compounds in the overlap area of the stable solid-phase regions of the two Pourbaix diagrams of Mn and Ni. This estimation is actually consistent with the fact that $MnNiO_3$ is stable in high pH region close to the OER potential. The above analysis suggests the possibility of long-term electrochemical stability of $MnNiO_3$ as an oxygen evolution photocatalyst in neutral-pH or alkaline solution.

In summary, we present the computational characterization of $MnNiO_3$, a promising oxygen-evolution photocatalyst. The magnetic ground state of $MnNiO_3$ is found to be ferrimagnetic, which is consistent with experimental observations. $MnNiO_3$ is found to be an indirect-band-gap semiconductor with an optimal band alignment to the HER and OER redox potentials. Furthermore, we find that the d-band splitting of both Mn and Ni atoms is crucial for obtaining the promising electronic structure properties as an oxygen evolution photocatalyst for water splitting. Lastly, the Pourbaix diagram analysis reveals that the compound is electrochemically stable in the relevant potential range at neutral pH or in alkaline solution providing possible long-term stability.

J. Y. was supported by the Joint Center for Artificial Photosynthesis through the U.S. Department of Energy, Office of Basic Energy Sciences, Materials Sciences and Engineering Division, under Contract No. DE-AC02-05CH11231. Q. Y., W. C. and A. J. were supported by the Materials Project (Grant No. EDCBEE), which is gratefully acknowledged for computing, infrastructure and software development support. Lastly, additional computational resources were provided by the Department of Energy through the National Energy Supercomputing Center (NERSC). Portions of this work were performed at the Molecular Foundry was supported by the Office of Science, Office of Basic Energy Sciences, of the U.S. Department of Energy under Contract No. DE-AC02-05CH11231.

Notes and references

[a] Joint Center for Artificial Photosynthesis, Lawrence Berkeley National Laboratory, Berkeley, CA 94720, United States.
[b] Environmental Energy Technologies Division, Lawrence Berkeley National Laboratory, Berkeley, California 94720, United States; E-mail: kapersson@lbl.gov
[c] Molecular Foundry, Lawrence Berkeley National Laboratory, Berkeley, California 94720, United States.
[d] Department of Physics, University of California, Berkeley, California 94720, United States.
[e] Kavli Energy NanoSciences Institute, Berkeley, CA 94720, United States

Electronic Supplementary Information (ESI) available: [details of magnetic calculations, Table S1, S2 and S3]. See DOI: 10.1039/c000000x

1. A. Fujishima and K. Honda, *Nature*, 1972, **238**, 37.
2. F. E. Osterloh, *Chem Mater*, 2008, **20**, 35.
3. S. Fukuzumi, D. C. Hong and Y. Yamada, *J Phys Chem Lett*, 2013, **4**.
4. K. Maeda and K. Domen, *J Phys Chem C*, 2007, **111**, 7851.
5. W. J. Yin, H. W. Tang, S. H. Wei, M. M. Al-Jassim, J. Turner and Y. F. Yan, *Phys Rev B*, 2010, **82**, 045106.
6. K. Sayama, K. Mukasa, R. Abe, Y. Abe and H. Arakawa, *Chem Commun*, 2001, 2416.
7. M. Pourbaix, *Atlas of electrochemical equilibria in aqueous solutions*, 2d English edn., National Association of Corrosion Engineers, Houston, Tex., 1974.
8. K. A. Persson, B. Waldwick, P. Lazic and G. Ceder, *Phys Rev B*, 2012, **85**, 235438.
9. A. Harriman, I. J. Pickering, J. M. Thomas and P. A. Christensen, *J Chem Soc Farad T 1*, 1988, **84**, 2795.
10. D. C. Hong, Y. Yamada, T. Nagatomi, Y. Takai and S. Fukuzumi, *J Am Chem Soc*, 2012, **134**.
11. D. C. Hong, Y. Yamada, A. Nomura and S. Fukuzumi, *Phys Chem Chem Phys*, 2013, **15**, 19125.
12. G. Kresse and J. Furthmuller, *Comp Mater Sci*, 1996, **6**, 15.
13. P. E. Blochl, *Phys Rev B*, 1994, **50**, 17953.
14. J. P. Perdew, K. Burke and M. Ernzerhof, *Phys Rev Lett*, 1996, **77**, 3865.
15. J. Heyd, G. E. Scuseria and M. Ernzerhof, *J Chem Phys*, 2003, **118**, 8207.
16. J. Heyd, G. E. Scuseria and M. Ernzerhof, *J Chem Phys*, 2006, **124**, 219906.
17. L. Wang, T. Maxisch and G. Ceder, *Phys Rev B*, 2006, **73**, 195107.
18. P. G. Moses, M. S. Miao, Q. M. Yan and C. G. Van de Walle, *J Chem Phys*, 2011, **134**, 084703.
19. W. H. Cloud, *Phys Rev*, 1958, **111**, 1046.
20. T. J. Swoboda, R. C. Toole and J. D. Vaughan, *J Phys Chem Solids*, 1958, **5**, 293.
21. Y. Y. Li, *Phys Rev*, 1956, **102**, 1015.
22. R. W. G. Wyckoff, *Crystal structures*, Interscience Publishers, New York, 1948.
23. E. F. Bertaut and F. Forrat, *J Appl Phys*, 1958, **29**, 247.
24. H. S. Jarrett and R. K. Waring, *Phys Rev*, 1958, **111**, 1223.
25. M. Pernet, J. C. Joubert and B. Ferrand, *Solid State Commun*, 1975, **16**, 503.
26. I. O. Troyanchuk, A. A. Shemyakov and V. K. Prokopenko, *Phys Status Solidi A*, 1989, **113**, K107.
27. M. Shishkin and G. Kresse, *Phys Rev B*, 2007, **75**, 235102.
28. M. van Schilfgaarde, T. Kotani and S. Faleev, *Phys Rev Lett*, 2006, **96**, 226402.
29. C. E. Patrick and F. Giustino, *J Phys-Condens Mat*, 2012, **24**, 202201.
30. R. F. Berger, C. J. Fennie and J. B. Neaton, *Phys Rev Lett*, 2011, **107**, 146804.
31. R. F. Berger and J. B. Neaton, *Phys Rev B*, 2012, **86**, 165211.
32. X. D. Wen, R. L. Martin, T. M. Henderson and G. E. Scuseria, *Chem Rev*, 2013, **113**, 1063.
33. A. Alkauskas, P. Broqvist, F. Devynck and A. Pasquarello, *Phys Rev Lett*, 2008, **101**, 106802.
34. W. Chen and A. Pasquarello, *Phys Rev B*, 2013, **88**, 119906.
35. W. H. Sun and G. Ceder, *Surf Sci*, 2013, **617**, 53.
36. D. O. Scanlon, C. W. Dunnill, J. Buckeridge, S. A. Shevlin, A. J. Logsdail, S. M. Woodley, C. R. A. Catlow, M. J. Powell, R. G. Palgrave, I. P. Parkin, G. W. Watson, T. W. Keal, P. Sherwood, A. Walsh and A. A. Sokol, *Nat Mater*, 2013, **12**, 798.
37. V. Stevanovic, S. Lany, D. S. Ginley, W. Tumas and A. Zunger, *Phys Chem Chem Phys*, 2014, **16**.
38. G. A. Parks, *Chem Rev*, 1965, **65**.
39. T. Mahmood, M. T. Saddique, A. Naeem, P. Westerhoff, S. Mustafa and A. Alum, *Ind Eng Chem Res*, 2011, **50**.
40. D. R. Huffman, R. L. Wild and M. Shinmei, *J Chem Phys*, 1969, **50**, 4092.
41. S. Hufner, J. Osterwalder, T. Riesterer and F. Hulliger, *Solid State Commun*, 1984, **52**, 793.
42. A. Jain, S. P. Ong, G. Hautier, W. Chen, W. D. Richards, S. Dacek, S. Cholia, D. Gunter, D. Skinner, G. Ceder and K. A. Persson, *Apl Mater*, 2013, **1**, 011002.
43. M. Pourbaix, *Atlas of electrochemical equilibria in aqueous solutions*, National Association of Corrosion Engineers, Houston, TX, 1974.
44. B. E. Douglas, D. H. McDaniel and J. J. Alexander, *Concepts and models of inorganic chemistry*, 3rd edn., Wiley, New York, 1994.
45. B. Beverskog and I. Puigdomenech, *Corros Sci*, 1997, **39**, 969.

